

The Chemistry of Water on Alumina Surfaces: Reaction Dynamics from First Principles

Kenneth C. Hass, William F. Schneider, Alessandro Curioni,
Wanda Andreoni*

Aluminas and their surface chemistry play a vital role in many areas of modern technology. The behavior of adsorbed water is particularly important and poorly understood. Simulations of hydrated α -alumina (0001) surfaces with *ab initio* molecular dynamics elucidate many aspects of this problem, especially the complex dynamics of water dissociation and related surface reactions. At low water coverage, free energy profiles established that molecularly adsorbed water is metastable and dissociates readily, even in the absence of defects, by a kinetically preferred pathway. Observations at higher water coverage revealed rapid dissociation and unanticipated collective effects, including water-catalyzed dissociation and proton transfer reactions between adsorbed water and hydroxide. The results provide a consistent interpretation of the measured coverage dependence of water heats of adsorption, hydroxyl vibrational spectra, and other experiments.

Aluminas [that is, the various allotropic forms of Al_2O_3 (1)] are well known to have a broad technological significance. The surface chemistry of aluminas plays a key role in their performance as catalysts and catalyst supports (2) and as dielectrics in microelectronics (3). Surface chemistry is also important in the adhesive bonding of lightweight aluminum alloys, which are increasingly replacing steel in the automobile industry (4), and it has been implicated in stratospheric ozone depletion through the effects of alumina particles in rocket exhaust (5). Despite this importance, many fundamentals of alumina surface chemistry are poorly understood. Experiments are often difficult to interpret because of the structural complexity of bulk aluminas and the problem of preparing reproducible well-characterized surfaces. Surface hydroxylation and dehydroxylation processes, in particular, are common, but their mechanisms, the conditions under which they occur, and their possible influence on measured properties are largely unknown. The work reported here addresses a number of these issues. The chosen alumina system was the thermodynamically stable phase α - Al_2O_3 . Water adsorption on the (0001) surface was investigated with parameter-free molecular dynamics (MD) simulations that are based on density functional theory (6–8). This study went beyond a determination of static structures and energetics and characterized the dynamics of several key surface reactions (9).

First principles investigations of reaction dynamics in condensed phases have only recently become possible (10) and are shown here to give new insights into alumina surface chemistry.

The intrinsic atomic structure of α - Al_2O_3 (0001) is generally agreed on, although experimental characterization of a hydrogen-free surface has proven to be challenging (3, 11). Electrostatic considerations as well as classical (12) and quantum (13) calculations indicate that the most favorable (0001) surface is terminated by a single plane of Al. Our calculations relied on a slab model (Fig. 1) with a supercell that was large enough to ensure computational accuracy and to allow us to study issues such as lateral mobility and the interactions between H_2O molecules.

The structure of the bare surface was optimized. In agreement with earlier studies, we found that the outermost Al atoms lie in nearly the same plane as the second-layer O atoms. Our predicted relaxations of the first four interlayer spacings were -82 , $+7$, -52 , and $+25\%$, which correspond to a surface relaxation energy of 1.89 J m^{-2} . Two recent experimental studies (11) have reported a slightly smaller relaxation of the first interlayer spacing (63 and 68%), but the simultaneous detection of surface hydrogen and the known difficulty of creating a OH-free alumina surface (14) probably account for much of this discrepancy. This conclusion is corroborated by the results discussed below.

The coordinatively unsaturated surface Al ions provide strong Lewis acid (electron-acceptor) sites for H_2O adsorption. We considered the low-coverage regime. Geometry optimizations for a single H_2O molecule produce three states: a metastable molecularly adsorbed state (Fig. 2A) and lower energy

1–2 and 1–4 dissociative states (Fig. 2, B and C). The calculated binding energies of 23.3, 33.2, and $32.5 \text{ kcal mol}^{-1}$, respectively, are within the expected energy range (14).

Water adsorption modifies the surface structure in all three states. The pattern and extent of surface relaxation are very different in the three cases. Molecular adsorption primarily pulls a single Al atom away from the surface, whereas dissociation has a more delocalized effect. For the atoms on the surface layer, the structural relaxation extends over two primitive cells of the (0001) surface (see Fig. 2, B and C). Most notably, in the 1–4 configuration, the surface Al atom that is bonded to the 4 site relaxes deep into the surface, thereby increasing its coordination and lowering its accessibility to water. For nonsurface atoms, the relaxation decays more rapidly into the slab in the 1–2 geometry than in the 1–4 geometry. Dissociation produces two distinct types of surface hydroxyl groups: $\text{O}_{\text{ads}}\text{H}$ and $\text{O}_\text{s}\text{H}$ (O_{ads} , water oxygen; O_s , surface oxygen). These groups differ in their O coordination numbers and thus in their vibrational frequencies and reactivities. As shown below, $\text{O}_\text{s}\text{H}$ is more likely to persist at higher H_2O coverages and to account in part for the presence of residual OH groups on calcined α - Al_2O_3 (14).

The extended nature of the above relaxations raise serious methodological concerns about alumina surface calculations that rely on smaller supercells or small isolated clusters. To clarify this point, we optimized the geometries for molecular and 1–2 dissociative H_2O adsorption also using small clusters (Al_8O_{12}) typically adopted in simulations of α - Al_2O_3 (0001) (15, 16). Large differences in calculated energetics and local structural relaxations were found in comparison to the above supercell results. In particular, because of edge effects, the 1–2 dissociated state with the highest binding energy (46 kcal mol^{-1}) in the cluster was heavily reconstructed and contained a broken Al– O_s bond.

Static calculations can provide only limited information on dynamical processes such as dissociation. In previous studies on other surfaces (17), the likelihood of H_2O dissociation was assessed entirely on the basis of energy barriers that were estimated from static calculations (TiO_2 and SnO_2) (18) or from observations made during short ($\sim 1 \text{ ps}$) unconstrained MD simulations [MgO (19) and TiO_2 (18)]. We examined the dynamics of H_2O dissociation on α - Al_2O_3 (0001) more directly by imposing geometrical constraints in first principles MD simulations (8, 20) that were run at room temperature. We applied this method to two distinct proton transfer reactions (1–2 and 1–4) and thereby determined their pathways and, by integrating their constraint forces (10), their entire free energy profiles (Fig. 3). The final states were

K. C. Hass and W. F. Schneider, Ford Research Laboratory, Dearborn, MI 48121–2053, USA. A. Curioni and W. Andreoni, IBM Research Division, Zurich Research Laboratory, 8803 Rüschlikon, Switzerland.

*To whom correspondence should be addressed. E-mail: and@zurich.ibm.com

REPORTS

both found to be ~ 10 kcal mol $^{-1}$ more favorable thermodynamically than the molecularly adsorbed state; similar values resulted from the above-mentioned energy minimizations, indicating that entropic contributions to the reaction free energies were small at 300 K.

Despite their thermodynamic similarity, the 1–2 and 1–4 dissociations differ substantially in the magnitudes of their free energy barriers of 6.6 and 2.2 kcal mol $^{-1}$, respectively. This difference reflects the qualitatively different nature of the two transition states: a four-membered ring for the 1–2 reaction and a much floppier six-membered ring for the 1–4 reaction. Minimizations near each transition state confirm that both energy and entropy contributions to the free energy barriers favor the 1–4 reaction. This can be attributed in part to its nearly linear O_{ads}–H–O_s hydrogen bond (21), which is not possible in the 1–2 reaction. Estimated rates (k) for the two reactions differ dramatically. Substituting the calculated barriers (ΔF) in the transition-state theory expression $k = (k_B T/h) \exp(-\Delta F/k_B T)$ yields $k = 0.16$ ps $^{-1}$ for unimolecular 1–4 dissociation but only $k = 10^{-4}$ ps $^{-1}$ for unimolecular 1–2 dissociation. This difference of three orders of magnitude strongly suggests that 1–4 reaction dissociation dominates the dissociation of preadsorbed H₂O.

The above results clearly establish that, in the low-coverage regime, H₂O dissociation is kinetically as well as thermodynamically favorable on defect-free α -Al₂O₃ (0001) at room temperature. The process is activated, but there is a kinetically preferred pathway with a small barrier. Our finding of well-

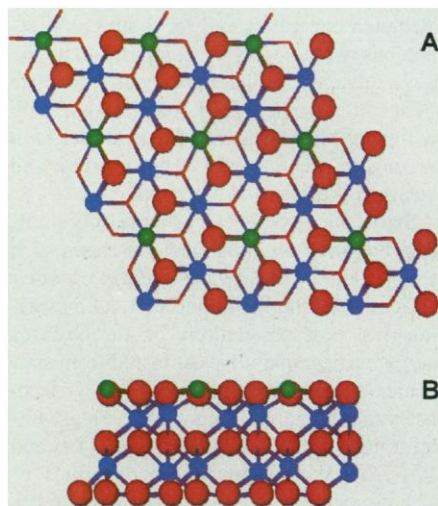


Fig. 1. (A) Top and (B) side view of the atoms within a single cell of the present model for a relaxed α -Al₂O₃ (0001) surface. Red, blue, and green spheres indicate O, interior Al, and surface Al atoms, respectively. The slab consists of a 3-unit cell by 3-unit cell hexagonal supercell containing 135 Al and O atoms in nine atomic layers. The vacuum between two slabs is ~ 10 Å.

defined 1–2 and 1–4 final states differs qualitatively from earlier classical MD simulations (22) for this system, which predicted that protons transferred by dissociation occupy hollow sites above three neighboring O_s atoms and diffuse easily along the surface at room temperature. Comparisons to earlier first principles calculations for H₂O on other oxide surfaces (18, 19) may not necessarily be conclusive because of the methodological differences discussed above [see also (17)]. In the case of MgO, only molecular adsorption was observed on the (100) surface in the absence of defects (19). This is presumably because of the lower Lewis acidity of five-fold-coordinated Mg as compared to three-fold-coordinated Al. On TiO₂ (110) and SnO₂ (110) (18), on the other hand, H₂O dissociation was claimed to be barrierless. Whether this result would persist in studies with larger supercells and constrained MD remains to be seen.

For the investigation of higher H₂O coverages, we performed unconstrained MD simulations beginning with nine H₂O molecules that were bound in different orientations to the nine surface Al atoms in each 3-unit cell by 3-unit cell supercell (Fig. 1) (8, 23). During ~ 1 ps of dynamics at ~ 250 K (see Fig. 4A), only one H₂O molecule was observed to undergo a spontaneous unimolecular 1–4 dissociation of the type discussed above. This observed rate of 1–4 dissociation is consistent with that estimated from Fig. 3. Also consistent is the fact that no analogous 1–2 dissociations were observed, despite what appeared to be many favorable opportunities. Thus, at least in the very early stages of reaction with H₂O, the unimolecular dissociation dynamics does not appear to be strongly perturbed by the presence of additional adsorbed molecules.

Fig. 2. Optimized geometries of (A) molecularly adsorbed, (B) 1–2 dissociated, and (C) 1–4 dissociated H₂O on α -Al₂O₃ (0001). Only atoms near the adsorption site are shown; Al and O atoms are colored as in Fig. 1, and H atoms are gray. Bond lengths are expressed in angstroms. Both molecular and dissociative adsorptions pull the Al surface atom that is bound to water oxygen (O_{ads}) away from the relaxed surface, to within 50 and 15%, respectively, of the bulk interlayer spacing. In the molecular case, the Al–O_{ads} bond is more than 0.2 Å longer than the bonds between the same Al and O_s. In both dissociated states, an Al–O_s bond to the O_sH site is elongated by ~ 0.15 Å. The root mean square (rms) displacements of the Al bound to O_{ads}, relative to the clean surface, are (A) 0.26, (B) 0.61, and (C) 0.53 Å. A large inward displacement of the surface Al atom bound to O_s in the 4 position in (C) is apparent; the rms displacement of this Al is 0.90 Å. Analyses of the electronic structures indicate that H₂O dissociates heterolytically, although a substantial charge redistribution accompanies the proton transfer.

The same MD run also revealed a number of other chemically significant events. In particular, collective behavior was observed in the vicinity of the Al–O_{ads} bond that broke during the run; one H₂O molecule “desorbed” early on from its molecular adsorption site and began to diffuse laterally along the surface in a precursor-like physisorbed state (24). The H₂O molecule then quickly became trapped by hydrogen bonding to a neighbor-

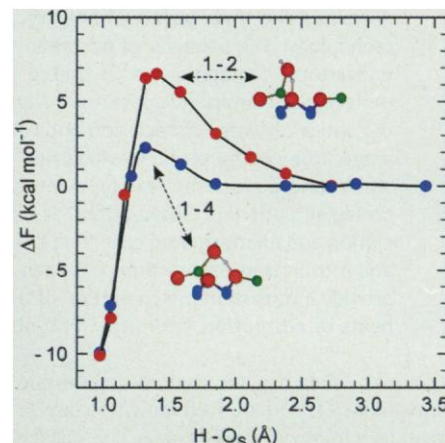
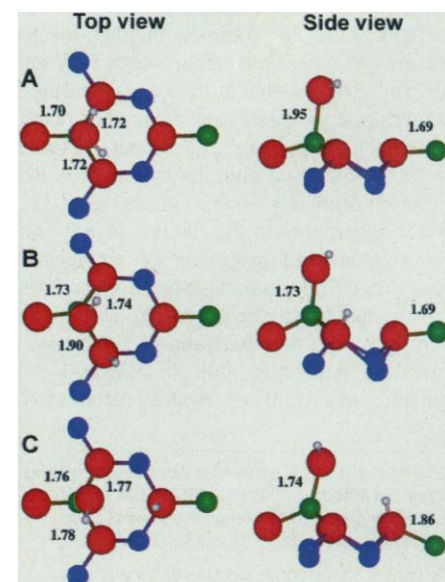


Fig. 3. Calculated free energy profiles at 300 K along proton transfer pathways between molecularly adsorbed H₂O and 1–2 (red circles) and 1–4 (blue circles) dissociated states. The reaction coordinate is the distance between the proton and the relevant O_s. The zero value of energy in each case corresponds to the initial state of molecularly adsorbed H₂O near its equilibrium position (Fig. 2A), with long H–O_s distances to the appropriate O_s sites. The final states correspond to H–O_s = 0.98 Å. The structures of the transition states were obtained by averaging the atomic coordinates over the constrained molecular dynamics simulation that was run in the vicinity of the two transition states. Surface Al atoms are represented by green spheres, and H atoms are gray.



ing molecule but subsequently freed itself and moved on to catalyze the 1–4 dissociation of a different adsorbed H₂O.

We also examined the details of the proton transfer processes involved in the observed unimolecular (Fig. 4B) and catalyzed (Fig. 4C) 1–4 dissociation reactions. The unimolecular reaction produced a rapid shift (from 0.18 to 0.3 ps) of one of the water protons (H_i) along a hydrogen bond from O_{ads} and O_s. After the reaction, the O_s–H_i bond remained vibrationally excited and was longer, on average, than the remaining O_{ads}–H bond, which contracted slightly upon dissociation. Weakly physisorbed H₂O catalyzes the 1–4 dissociation reaction shown in Fig. 4C by allowing the synchronous transfer of two protons along two neighboring hydro-

gen bonds. Hydrogen bonding to the O_s site clearly manifests itself in an increase of the amplitude of O–H_i, which stretched for 100 fs until the proton was transferred. The second transfer (of H₂ from O_{ads} to O) was completed within ~40 fs of the first. Both hydrogen bonds to the newly formed H₂O molecule eventually broke, allowing this molecule to diffuse and yielding the same net result as shown in Fig. 4B. Synchronous proton transfer reactions of this type are expected in many systems that contain multiple hydrogen bonds within closed topological loops (21), but to our knowledge, this was the first direct observation of such a reaction in a first principles dynamical simulation.

The dissociation event and the distinct nature of the two OH groups produced are also reflected in the frequencies of the OH stretching modes derived from the MD trajectories (25). In molecularly adsorbed H₂O molecules, they lie in the range of 3450 to 3650 cm⁻¹, whereas for O_s–H and O_{ads}–H, they lie at ~3430 and 3780 cm⁻¹, respectively. The latter value is in excellent agreement with a high-frequency peak that is often observed on hydroxylated aluminas and confirms the usual assignment of this peak to terminal OH on fourfold-coordinated Al (2, 26). Vibrations of O_s–H and molecularly adsorbed H₂O are more difficult to identify in experimental spectra, which often exhibit a variety of broad features in the range of 3400 to 3600 cm⁻¹, with intensities that depend strongly on sample conditions and temperature.

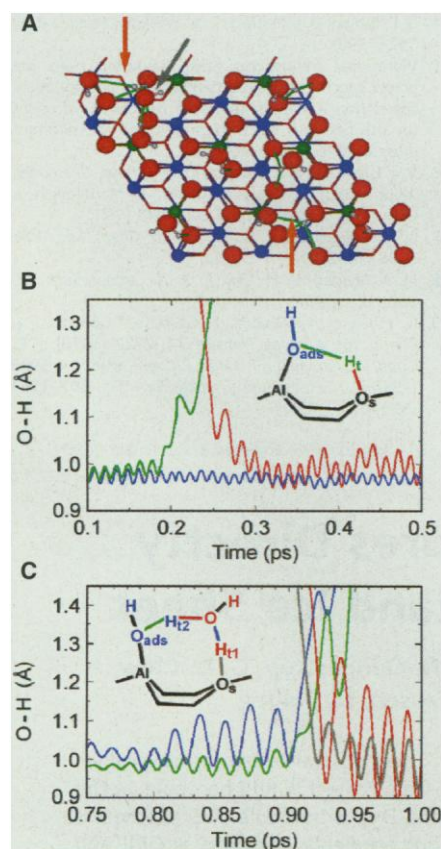


Fig. 4. (A) Snapshot of the 300 K dynamical simulation of an α -Al₂O₃(0001) surface plus nine H₂O molecules, taken after ~1 ps. Colors are the same as in Fig. 1. Green lines indicate hydrogen bonds (defined with a cutoff radius of 2.2 Å). Orange arrows indicate 1–4 chemisorbed species, and the gray arrow indicates a weakly physisorbed H₂O molecule. Temporal variations in the O–H bond lengths during (B) unimolecular 1–4 and (C) H₂O-catalyzed 1–4 dissociation reactions observed in simulations. Curves are color-coded to bonds shown in insets. The reaction (C) is catalyzed by weakly physisorbed H₂O, which is shown in red. The two O–H_i distances cross when the O_{ads}–H_i–O_s angle is close to 180° and the O_{ads}–O_s distance is close to a minimum (2.5 Å).

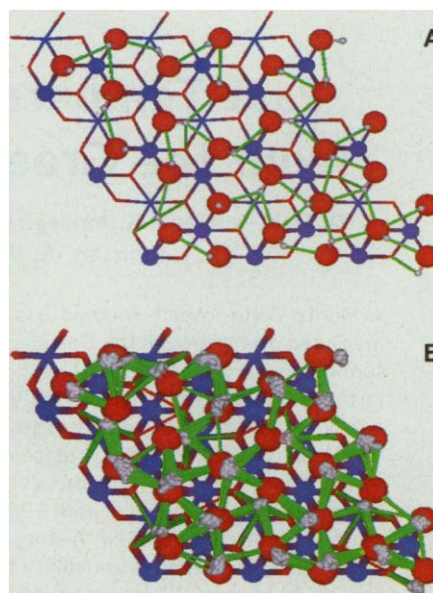


Fig. 5. Fully hydroxylated α -Al₂O₃(0001) surface obtained by replacing surface Al in Fig. 1 with three H atoms (gray spheres). (A) Initial configuration and (B) superposition of configurations sampled at regular intervals of 1 ps of dynamics. The green lines correspond to hydrogen bonds (as in Fig. 4A); the large number of these bonds illustrates the complex dynamical nature of this surface.

Additional MD simulations revealed spontaneous (and therefore nearly barrierless) proton transfer reactions between molecularly adsorbed H₂O and O_{ads}H groups on neighboring Al sites. These reactions, which are thermoneutral, provide a mechanism for proton diffusion that may contribute to the dynamical behavior observed in ²⁷Al nuclear magnetic resonance studies (27) of partially hydroxylated alumina surfaces.

With only the reactions identified so far, complete hydroxylation of α -Al₂O₃(0001) would result in one O_{ads}H on each surface Al and one O_sH for every three surface O atoms, for a coverage of ~10 OH per square nanometer. Calculations for this configuration yield an average H₂O chemisorption energy of 27.5 kcal mol⁻¹. Assuming a linear decrease in dissociative adsorption energy from the 33 kcal mol⁻¹ found at low coverages, we extracted a value of 22 kcal mol⁻¹ for the ninth H₂O molecule in each supercell. Test calculations indicated that the molecular adsorption energy also decreased with coverage, so that dissociation remained favored throughout this range. The present results suggest a consistent interpretation of measured H₂O heats of chemisorption on nanocrystalline α -Al₂O₃ (14). Three different behavior regimes were clearly observed: Below 5 OH per square nanometer, the differential heat of H₂O adsorption was >44 kcal mol⁻¹; from 5 to 10 OH per square nanometer, the differential heat decreased nearly linearly to ~37 kcal mol⁻¹; and above 10 OH per square nanometer, the differential heat decreased nearly exponentially (14). Although it is difficult to make quantitative comparisons (because of the presence of other crystal faces and other experimental uncertainties), it is likely that the low-coverage regime is dominated by surface defects, the intermediate regime corresponds to the intrinsic adsorption processes studied in the present work, and the high-coverage regime involves many competing processes, including hydrogen bonding to preadsorbed H₂O and multiple H₂O adsorption on both first- and second-layer Al. We think that the consistency of the present results with the observed decrease in adsorption energy in the intrinsic regime and the abrupt change in behavior at a coverage of 10 OH per square nanometer are particularly important.

At coverages > 10 OH per square nanometer, many of the surface Al–O_s bonds were highly strained or broken, making some second-layer Al more accessible to H₂O. Further MD simulations with 10 dissociated H₂O molecules per supercell (with one O_{ads}H on a second-layer Al and the transferred proton on an adjacent O_s site) showed that an interesting rearrangement can occur: The interior O_{ads}H replaces its neighboring O_sH, whereas the O_sH tilts up and becomes singly coordi-

nated to a surface Al, providing a mechanism for the interchange of O_s and O_{ads} . These results also provide evidence for incipient $Al(OH)_3$ formation on the surface. The ultimate structure of the heavily hydrated surface is clearly very complicated and may depend strongly on sample history. It is possible that the $Al(OH)_3$ species can be removed completely (perhaps starting near steps or other defects), leaving a less reactive surface that is completely O_3H -terminated, which is similar to the known surfaces of aluminum hydroxides (1).

An idealized model for fully hydroxylated $\alpha-Al_2O_3(0001)$ (28) replaces each surface Al with three H atoms (Fig. 5A), yielding a coverage >15 OH per square nanometer. Room-temperature MD simulations of this model revealed a complex dynamic structure (Fig. 5B), with one out of every three OH groups, on average, lying parallel to the surface because of in-plane hydrogen bonding. Calculated O-H vibrational spectra (25) yielded two broad peaks at ~ 3470 and 3650 cm^{-1} , with the peak at ~ 3470 cm^{-1} corresponding to in-plane OH groups. The peak at ~ 3650 cm^{-1} is close to the single peak (3720 to 3733 cm^{-1}) that is observed in most measurements on hydroxylated $\alpha-Al_2O_3(0001)$ (29) and to the range that is generally assigned to bridging OH groups (2, 26). The peak at ~ 3470 cm^{-1} is red-shifted by hydrogen bonding and is generally not seen in single-crystal experiments, perhaps because of selection rules or because it is too broad. Our finding of two peaks split by 200 cm^{-1} contradicts all previous classifications of OH vibrations (and subsequent cluster modeling) (2) on aluminas, which assume that all OH groups with the same coordination of O and neighboring Al have the same frequency. By this criterion, all of the surface OH groups in Fig. 5 are equivalent; however, their stretch frequencies clearly depend also on longer range environmental effects.

The present investigation of $\alpha-Al_2O_3(0001)$ has elucidated several aspects of the complex interactions of H_2O with an alumina surface, especially the dynamics of dissociation reactions at low and high coverages. On the basis of these results, a consistent interpretation of a diverse set of experimental data on hydroxylated alumina surfaces begins to emerge.

References and Notes

1. K. Wefers and C. Misra, *Alcoa Tech. Pap.* 19 (revised) (Alcoa Laboratories, St. Louis, MO, 1987).
2. H. Knözinger and P. Ratnasamy, *Catal. Rev. Sci. Eng.* **17**, 31 (1978).
3. M. Gautier et al., *J. Am. Ceram. Soc.* **77**, 323 (1994).
4. P. de Sainte Claire, K. C. Hass, W. F. Schneider, W. L. Hase, *J. Chem. Phys.* **106**, 7331 (1997).
5. G. N. Robinson, Q. Dai, A. Freedman, *J. Phys. Chem. B* **101**, 4940 (1997).
6. R. Car and M. Parrinello, *Phys. Rev. Lett.* **55**, 2471 (1985).
7. The gradient-corrected exchange-correlation [Bernstein, Lee, Yang, and Primakoff (BLYP)] functional

- used here is from A. D. Becke [*Phys. Rev. A* **38**, 3098 (1988)] and C. Lee, W. Yang, and R. Parr [*Phys. Rev. B* **37**, 785 (1988)]. Norm-conserving numerical pseudopotentials were generated for Al and O with the procedure of N. Troullier and J. L. Martins [*ibid.* **43**, 1993 (1991)], and a local analytic pseudopotential was derived for H. This is essentially a softened Coulomb potential with a core radius of 0.25 atomic units. Electron wave functions are expanded in a plane-wave basis set with an energy cutoff of 70 rydbergs (Ry). We used the Car-Parrinello Molecular Dynamics code in the parallelized 2.5 version (developed by J. Hutter and copyrighted by IBM, Armonk, NY). All calculations were performed on a 32-node IBM RS6000 SP at the IBM Watson Research Laboratory (Yorktown Heights, NY).
8. In the MD runs, a value of 400 au was used for the fictitious electron mass of the Car-Parrinello Lagrangian multipliers (6), and each hydrogen molecule was replaced by deuterium to improve the separation between electronic and ionic degrees of freedom. The time step in the Verlet algorithm for the integration of the equations of motions was ~ 0.1 fs.
 9. The importance of chemical reaction dynamics in general has recently been highlighted in a special issue of *Science* [Reaction Dynamics, *Science* **279**, 1875–1895 (1998)].
 10. A. Curioni et al., *J. Am. Chem. Soc.* **119**, 7218 (1997).
 11. V. E. Puchin et al., *Surf. Sci.* **370**, 190 (1997); J. Ahn and J. W. Rabalais, *ibid.* **388**, 121 (1997).
 12. See, for example, S. Blonski and S. H. Garofalini, *ibid.* **295**, 263 (1993).
 13. See, for example, M. Causa, R. Dovesi, C. Pisani, C. Roetti, *ibid.* **215**, 259 (1989); I. Manassidis, A. De Vita, M. J. Gillan, *Surf. Sci. Lett.* **285**, L517 (1993); I. Frank, D. Marx, M. Parrinello, *J. Chem. Phys.* **104**, 8143 (1996).
 14. J. M. McHale, A. Auroux, A. J. Perrotta, A. Navrotsky, *Science* **277**, 788 (1997). For earlier work, see P. A. Thiel and T. E. Madey, *Surf. Sci. Rep.* **7**, 211 (1987) and references therein.
 15. J. M. Wittbrodt, W. L. Hase, H. B. Schlegel, *J. Phys. Chem. B* **102**, 6539 (1998).
 16. K. C. Hass, W. F. Schneider, A. Curioni, W. Andreoni, in preparation.
 17. Earlier calculations used much smaller supercells than the present work. Such studies were therefore limited

in their ability to provide accurate adsorbate structures and energies and to study the H_2O coverage dependence and phenomena such as collective effects and surface diffusion.

18. J. Goniakowski and M. J. Gillan, *Surf. Sci.* **350**, 145 (1996); P. J. D. Lindan, N. M. Harrison, J. M. Holdender, M. J. Gillan, *Chem. Phys. Lett.* **261**, 246 (1996); P. J. D. Lindan, N. M. Harrison, M. J. Gillan, *Phys. Rev. Lett.* **80**, 762 (1998).
19. W. Langel and M. Parrinello, *J. Chem. Phys.* **103**, 3240 (1995).
20. Lagrange multipliers were introduced to constrain the relevant H-O₂ distance, and the average constraint forces were determined from constant temperature simulations [S. Nosé, *J. Chem. Phys.* **81**, 511 (1984); W. G. Hoover, *Phys. Rev. A* **31**, 1695 (1985)] of at least 0.2 ps.
21. S. Scheiner, in *Proton Transfer in Hydrogen-Bonded Systems*, T. Bountis, Ed. (Plenum, New York, 1992), p. 29.
22. S. Blonski and S. H. Garofalini, *J. Phys. Chem.* **100**, 2201 (1996).
23. The temperature was not controlled but was increased slowly from ~ 100 to ~ 350 K. The system was then allowed to evolve for a time interval of >1 ps. The average temperature was 250 K.
24. D. E. Brown, D. J. Moffatt, R. A. Wolkow, *Science* **279**, 542 (1998).
25. Vibrational frequencies were estimated from the power spectra of the (partial) velocity-velocity autocorrelation functions and were rescaled to account for the fictitious electronic mass and the different mass used for the proton.
26. V. I. Lygin and I. S. Muzyka, *Russ. J. Phys. Chem.* **69**, 1829 (1995); A. Tsyganenko and P. Mardilovich, *J. Chem. Soc. Faraday Trans.* **92**, 4843 (1996).
27. B. A. Huggins and P. D. Ellis, *J. Am. Chem. Soc.* **114**, 2098 (1992).
28. M. A. Nygren, D. H. Gay, C. R. A. Catlow, *Surf. Sci.* **380**, 113 (1997).
29. C. Morterra, G. Ghiotti, E. Garrone, F. Boccuzzi, *J. Chem. Soc. Faraday Trans.* **1** **72**, 2722 (1976); J. G. Chen, J. E. Crowell, J. T. Yates, *J. Chem. Phys.* **84**, 5906 (1986); V. Coustet and J. Jupille, *Surf. Sci.* **307**, 1161 (1994).

11 August 1998; accepted 3 September 1998

Past Temperatures Directly from the Greenland Ice Sheet

D. Dahl-Jensen,* K. Mosegaard, N. Gundestrup, G. D. Clow, S. J. Johnsen, A. W. Hansen, N. Balling

A Monte Carlo inverse method has been used on the temperature profiles measured down through the Greenland Ice Core Project (GRIP) borehole, at the summit of the Greenland Ice Sheet, and the Dye 3 borehole 865 kilometers farther south. The result is a 50,000-year-long temperature history at GRIP and a 7000-year history at Dye 3. The Last Glacial Maximum, the Climatic Optimum, the Medieval Warmth, the Little Ice Age, and a warm period at 1930 A.D. are resolved from the GRIP reconstruction with the amplitudes -23 kelvin, $+2.5$ kelvin, $+1$ kelvin, -1 kelvin, and $+0.5$ kelvin, respectively. The Dye 3 temperature is similar to the GRIP history but has an amplitude 1.5 times larger, indicating higher climatic variability there. The calculated terrestrial heat flow density from the GRIP inversion is 51.3 milliwatts per square meter.

Measured temperatures down through an ice sheet relate directly to past surface temperature changes. Here, we use the measurements from two deep boreholes on the Greenland Ice Sheet to reconstruct past temperatures. The GRIP ice core ($72.6^\circ N$, $37.6^\circ W$) was successfully recovered in 1992 (1, 2), and the

3028.6-m-deep liquid-filled borehole with a diameter of 13 cm was left undisturbed. Temperatures were then measured down through the borehole in 1993, 1994, and 1995 (3, 4). We used the measurements from 1995 (Fig. 1) (4), because there was no remaining evidence of disturbances from the drilling and